



**HAL**  
open science

# A New Approach to 3D ICP Covariance Estimation for Mobile Robotics

Martin Brossard, Silvère Bonnabel, Axel Barrau

► **To cite this version:**

Martin Brossard, Silvère Bonnabel, Axel Barrau. A New Approach to 3D ICP Covariance Estimation for Mobile Robotics. 2019. hal-02284430v1

**HAL Id: hal-02284430**

**<https://hal.science/hal-02284430v1>**

Preprint submitted on 12 Sep 2019 (v1), last revised 21 Jan 2020 (v2)

**HAL** is a multi-disciplinary open access archive for the deposit and dissemination of scientific research documents, whether they are published or not. The documents may come from teaching and research institutions in France or abroad, or from public or private research centers.

L'archive ouverte pluridisciplinaire **HAL**, est destinée au dépôt et à la diffusion de documents scientifiques de niveau recherche, publiés ou non, émanant des établissements d'enseignement et de recherche français ou étrangers, des laboratoires publics ou privés.

# A New Approach to 3D ICP Covariance Estimation for Mobile Robotics

Martin BROSSARD\*, Silvère BONNABEL\* and Axel BARRAU†

\*MINES ParisTech, PSL Research University, Centre for Robotics, 60 Boulevard Saint-Michel, 75006 Paris, France

†Safran Tech, Groupe Safran, Rue des Jeunes Bois-Châteaufort, 78772, Magny Les Hameaux Cedex, France

**Abstract**—In mobile robotics, scan matching of point clouds using Iterative Closest Point (ICP) allows estimating sensor displacements. It may prove important to assess the associated uncertainty about the obtained rigid transformation, especially for sensor fusion purposes. In this paper we propose a novel approach to 3D ICP covariance computation that accounts for all the sources of errors as listed in Censi’s pioneering work, namely wrong convergence, underconstrained situations, and sensor noise. Our approach builds on two facts. First, ICP is not a standard sensor: owing to wrong convergence the concept of ICP covariance *per se* is actually meaningless, as the dispersion in the ICP outputs may largely depend on the accuracy of the initialization, and is thus inherently related to the prior uncertainty on the displacement. We capture this using the unscented transform, which also reflects correlations between initial and final uncertainties. Then, assuming white sensor noise leads to overoptimism: ICP is biased, owing to e.g. calibration biases, which we account for. Our solution is tested on publicly available real data ranging from structured to unstructured environments, where our algorithm predicts consistent results with actual uncertainty, and compares very favorably to previous methods. We finally demonstrate the benefits of our method for pose-graph localization, where our approach improves accuracy and robustness of the estimates.

**Index Terms**—ICP, covariance estimation, localization

## I. INTRODUCTION

Point clouds and the Iterative Closest Point (ICP) algorithm play a crucial role for localization and mapping in modern mobile robotics [1]. ICP computes an estimate

$$\hat{\mathbf{T}}_{\text{icp}} = \text{icp}(\mathcal{P}, \mathcal{Q}, \hat{\mathbf{T}}_{\text{odo}}) \quad (1)$$

of the 3D rigid transformation  $\mathbf{T} \in SE(3)$  that aligns a reference point cloud  $\mathcal{P}$  to a reading point cloud  $\mathcal{Q}$  (or more generally a model or a surface). The algorithm starts with a first transformation estimate  $\hat{\mathbf{T}}_{\text{odo}} \in SE(3)$ , and repeats - until convergence - point association and least-square minimization. Note that in mobile robotics initialization  $\hat{\mathbf{T}}_{\text{odo}}$  is naturally provided by odometry [2,3], based on wheel speeds, inertial sensors, or stereo vision. The point association matches points between the two clouds by generally associating each point of  $\mathcal{Q}$  to its closest point in  $\mathcal{P}$ . Then, the algorithm minimizes a metric [4] between the matched points that provides an update of the current estimate  $\hat{\mathbf{T}}_{\text{icp}}$ . In spite of thresholding on point density, random sub-sampling and weighting that are broadly used during the alignment of point clouds, a.k.a. registration, ICP is subject to errors stemming from sensor noises, underconstrained environments that result

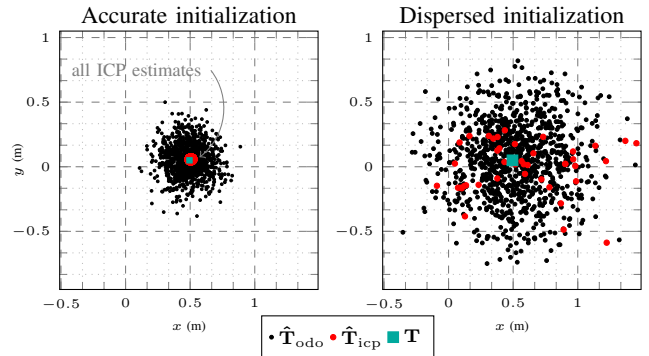


Fig. 1. Horizontal translation according to ICP ( $\hat{\mathbf{T}}_{\text{icp}}$ , red dots) for various initial estimates ( $\hat{\mathbf{T}}_{\text{odo}}$ , black dots) and ground-truth ( $\mathbf{T}$ , square) for registering two scans of the real data sequence *Stairs* of [8], where we sample 1000 initial estimates from two distributions reflecting accurate (left) and dispersed (right) ICP initialization and that respectively correspond to the easy and medium scenarios of [9]. We see the uncertainty on the ICP estimate, that is, dispersion of red points, wholly depends on the accuracy of initialization. There is no “covariance of ICP” *per se*.

in unobservable directions, and the fact that the algorithm is prone to local minima [5]–[7].

### A. Sources of ICP Uncertainty

The pioneering work of Censi [6] identifies the following sources of error for ICP registration: wrong convergence (not handled by Censi’s formula), underconstrained situations, and sensor noise. As indicated by preliminary remarks in [10,11] we believe a fourth important source is missing: the one that stems from sensor biases. In the present paper we consider indeed the following sources of error:

1) *Initial Transformation*: ICP is subject to error due to wrong initialization that makes the algorithm converge to a local minimum out of the attraction basin of the true solution, as largely observed in practice, see e.g. [7,12] and Figure 1 (right). In practice it often proves to be the dominant error.

2) *Sensor White Noise*: each *point* measured in  $\mathcal{P}$  and  $\mathcal{Q}$  is affected by an *independent* random sensor noise of centimetric magnitude which is a function of point depth and beam angle [5,13].

3) *Sensor Bias Noise*: the observed points in  $\mathcal{P}$  or in  $\mathcal{Q}$  share common errors that stem from: temperature drift effect, i.e. stability of the laser [13]; observed material [5]; incidence and beam angles resulting in large bias [14]; or wrong calibration, e.g. [15] found a distortion of 0.22 deg of

the scan point clouds due to intrinsic calibration process. This *correlated* noise, a.k.a. bias, strictly limits the confidence we may have in the ICP estimate. To our best knowledge this is often omitted with a few exceptions: e.g., [14] removes bias on point measurements due to sensor beam angle, and preliminary ideas may be found in [10,11].

4) *Intern ICP Algorithm*: ICP is generally configured with random processes [1], e.g. sub-sampling, such that two solutions with exactly the same inputs would differ.

In the following we address uncertainty coming from 1), 2) and 3) and do not consider 4), which should be marginal.

### B. Brief Literature Review

Various approaches exist for estimating the covariance of the ICP algorithm, each of which being a trade-off between accuracy and execution time. Monte-Carlo algorithms, e.g. [12,16], sample noisy scans (from a reference scan) and ICP initializations to compute a large number of ICP registration results, define the covariance of the sampled results as the covariance estimation, and use the estimated covariance for all future registration with the reference scan, thus getting a covariance function of the reference scan only. Another category of covariance estimation methods relies on closed-form expressions [6,17]–[19], whose underlying assumption consists in linearizing the objective function used in ICP around the convergence point, ruling out the possibility for wrong convergence and the uncertainty that stems from it. Albeit still used in practice, Censi’s pioneering formula [6] is widely considered as overoptimistic, see e.g. [20] for pose-graph based on ICP measurements. Recently, [7] leveraged learning based approaches to estimate ICP uncertainty stemming from inaccurate ICP initialization.

### C. Contributions and Paper’s Organization

Our approach introduced in Section II extends existing works in three ways: 1) we consider ICP uncertainty coming both from sensor errors and ICP initialization (wrong convergence). 2) we raise an important point which is that ICP uncertainty in itself is meaningless as it is inherently related to uncertainty in the initialization point (unless there is a global minimum). This is supported by experiments displayed in Figure 1. We address this problem by outputting a covariance matrix of larger dimension that also reflects the correlation between ICP final and initial estimates. And 3) we estimate in Section III the ICP uncertainty combining a closed-form expression using [6,17] accounting for sensor biases, and deterministic derivative-free methods using the unscented transform of [21,22], which comes at a lower computational cost than Monte-Carlo runs.

Besides, we evaluate and compare our approach on the dataset of [8] in Section IV, where our approach obtains consistent estimates and achieves better results than existing methods. Building upon our larger covariance matrix, we derive in Section V a specific pose-graph where factors account for correlations between odometry and ICP, see Figure 2. It leads to more accurate and robust results compared to standard pose-graph methods. The code to reproduce the results of the paper

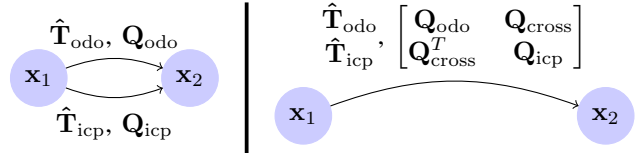


Fig. 2. ICP computes rigid transformation  $\hat{\mathbf{T}}_{\text{icp}}$  that may serve as a laser odometry sensor which is combined with other types of odometry based on inertial sensors and/or differential wheel speeds, that provide relative transformation  $\hat{\mathbf{T}}_{\text{odo}}$  [2,3]. To perform fusion for localization one may use, e.g., pose-graph optimization like GTSAM [23] or  $g^2o$  [24], that requires evaluating odometry uncertainty  $\mathbf{Q}_{\text{odo}}$  and ICP uncertainty  $\mathbf{Q}_{\text{icp}}$ . Whereas the naive approach consists in considering  $\hat{\mathbf{T}}_{\text{icp}}$  and  $\hat{\mathbf{T}}_{\text{odo}}$  as independent measurements, we note ICP estimate *is* a function of odometry estimate, see (1), since our best guess for ICP initialization is  $\hat{\mathbf{T}}_{\text{odo}}$ , see also [1,7], and  $\hat{\mathbf{T}}_{\text{icp}}$  and  $\hat{\mathbf{T}}_{\text{odo}}$  are thus *correlated*. In the above diagram, poses  $\mathbf{x}_1$  and  $\mathbf{x}_2$  are linked by odometry (IMU or wheel speeds) and ICP. Our algorithm takes  $\hat{\mathbf{T}}_{\text{odo}}$  and  $\mathbf{Q}_{\text{odo}}$  as inputs and computes ICP covariance  $\mathbf{Q}_{\text{icp}}$  of  $\hat{\mathbf{T}}_{\text{icp}}$  but also cross-covariance  $\mathbf{Q}_{\text{cross}}$  of  $\hat{\mathbf{T}}_{\text{icp}}$  and  $\hat{\mathbf{T}}_{\text{odo}}$ . In terms of graph, we replace two links by one with larger associated covariance matrix.

is made publicly available at: <https://github.com/CAOR-MINES-ParisTech/3d-icp-cov>.

Throughout the article, we configure the ICP as suggested in [9] with a point-to-plane error metric.

## II. PROPOSED APPROACH

In this section we introduce a novel approach to ICP uncertainty.

### A. Statistical Insight

Assume a wholly unknown noise free vector  $\mathbf{x}$  must be estimated from two noisy measurements  $\mathbf{y}_1 = \mathbf{x} + \mathbf{w}_1$  and  $\mathbf{y}_2 = \mathbf{x} + \mathbf{J}\mathbf{w}_1 + \mathbf{G}\mathbf{w}_2$ , where  $\mathbf{w}_1$  and  $\mathbf{w}_2$  are independent centered Gaussian noises with covariance matrices  $\mathbf{Q}_1$  and  $\mathbf{Q}_2$ . To assess uncertainty about the maximum likelihood estimate of  $\mathbf{x}$  in the light of  $\mathbf{y}_1$  and  $\mathbf{y}_2$  we write:

$$\begin{bmatrix} \mathbf{y}_1 \\ \mathbf{y}_2 \end{bmatrix} = \mathbf{A}\mathbf{x} + \mathbf{w}, \quad \text{cov}(\mathbf{w}) = \begin{bmatrix} \mathbf{Q}_1 & \mathbf{Q}_1\mathbf{J}^T \\ \mathbf{J}\mathbf{Q}_1 & \mathbf{J}\mathbf{Q}_1\mathbf{J}^T + \mathbf{G}\mathbf{Q}_2\mathbf{G}^T \end{bmatrix}, \quad (2)$$

where  $\mathbf{A} = [\mathbf{1} \ \mathbf{1}]^T$ . The covariance matrix  $\mathbf{P}$  of the maximum likelihood estimate of  $\mathbf{x}$  satisfies  $\mathbf{P}^{-1} = \mathbf{A}^T \text{cov}(\mathbf{w})^{-1} \mathbf{A}$ . We also note that  $\text{cov}(\mathbf{y}_2) = \mathbf{J}\mathbf{Q}_1\mathbf{J}^T + \mathbf{G}\mathbf{Q}_2\mathbf{G}^T$ .

### B. Uncertainty Representation for Poses

Since the true pose  $\mathbf{T}$  and estimate  $\hat{\mathbf{T}}_{\text{icp}}$  live in  $SE(3)$  which is not a vector space, we opt for the uncertainty representation (named concentrated Gaussian) [22,25]–[29]

$$\mathbf{T} = \exp(\boldsymbol{\xi}) \hat{\mathbf{T}}, \quad \text{where } \boldsymbol{\xi} \sim \mathcal{N}(\mathbf{0}, \mathbf{Q}), \quad (3)$$

with  $\exp(\cdot)$  the exponential map in  $SE(3)$ ,  $\boldsymbol{\xi} \in \mathbb{R}^6$  a random variable, and  $\mathcal{N}(\cdot, \cdot)$  the standard Gaussian distribution in  $\mathbb{R}^6$ . The pose covariance matrix is  $\mathbf{Q} \in \mathbb{R}^{6 \times 6}$  and  $\hat{\mathbf{T}}$  the “best” or average estimate. We note this distribution  $\mathbf{T} \sim \mathcal{N}_R(\hat{\mathbf{T}}, \mathbf{Q})$ .

### C. Proposed Uncertainty Simple Model

Suppose  $\mathbf{T}$  denotes the true transformation. Assume  $\mathbf{T} = \exp(\boldsymbol{\xi}_{\text{odo}})\hat{\mathbf{T}}_{\text{odo}}$ , where  $\hat{\mathbf{T}}_{\text{odo}}$  denotes a first available estimate stemming from odometry, either based on an Inertial Measurement Unit (IMU), wheel speeds, stereo vision, or pure Brownian motion assumption in the absence of odometry sensor, and  $\text{cov}(\boldsymbol{\xi}_{\text{odo}}) = \mathbf{Q}_{\text{odo}}$  its (known) associated uncertainty. Note that as  $\boldsymbol{\xi}_{\text{odo}}$  is centered we may write  $\exp(\boldsymbol{\xi}_{\text{odo}})\mathbf{T} = \hat{\mathbf{T}}_{\text{odo}}$  without changing  $\mathbf{Q}_{\text{odo}}$ . ICP's final estimate  $\hat{\mathbf{T}}_{\text{icp}}$  from (1) may be actually rewritten as a function  $\hat{\mathbf{T}}_{\text{icp}} = f(\hat{\mathbf{T}}_{\text{odo}}, \mathbf{w}_{\text{sensor}})$ , where  $\mathbf{w}_{\text{sensor}}$  denotes scan sensor noise that induces small fluctuations in the point clouds  $\mathcal{P}, \mathcal{Q}$ , and also that stems from unknown biases which depend on the calibration process and drift with temperature [13]. Thus the ICP estimate has the following form

$$\hat{\mathbf{T}}_{\text{icp}} = f(\exp(\boldsymbol{\xi}_{\text{odo}})\mathbf{T}, \mathbf{w}_{\text{sensor}}). \quad (4)$$

Assuming ICP's final estimate  $\hat{\mathbf{T}}_{\text{icp}}$  to be also distributed as  $\mathbf{T} \sim \mathcal{N}_R(\hat{\mathbf{T}}_{\text{icp}}, \hat{\mathbf{Q}}_{\text{icp}})$ , (4) rewrites as

$$\boldsymbol{\xi}_{\text{icp}} = g(\boldsymbol{\xi}_{\text{odo}}, \mathbf{w}_{\text{sensor}}), \quad (5)$$

where  $g(\boldsymbol{\xi}, \mathbf{w}) := -\log(\mathbf{T}^{-1}f(\exp(\boldsymbol{\xi})\mathbf{T}, \mathbf{w}))$  with  $\log(\cdot)$  the logarithm map of  $SE(3)$  as defined in [26].

“Censi-like” formulas address only the dispersion owed to  $\mathbf{w}_{\text{sensor}}$  and provide a way to linearize  $g(\cdot, \cdot)$  with respect to its second variable assuming correct convergence. This amounts to postulating  $\boldsymbol{\xi}_{\text{odo}} = \mathbf{0}$  and closed formulas yield approximation  $g(\mathbf{0}, \mathbf{w}_{\text{sensor}}) \approx g(\mathbf{0}, \mathbf{0}) + \mathbf{G}\mathbf{w}_{\text{sensor}}$ . In turn this yields a covariance matrix (at convergence)  $\hat{\mathbf{Q}}_{\text{conv}}^{\text{at}} = \mathbf{G}\mathbf{Q}_{\text{sensor}}\mathbf{G}^T$  with  $\mathbf{Q}_{\text{sensor}} = \text{cov}(\mathbf{w}_{\text{sensor}})$  having centimetric magnitude.

By contrast, the function relating  $\boldsymbol{\xi}_{\text{odo}}$  to  $\boldsymbol{\xi}_{\text{icp}}$  (assuming  $\mathbf{w}_{\text{sensor}}$  to be fixed) is strongly dependent on the magnitude of  $\boldsymbol{\xi}_{\text{odo}}$  and cannot be captured by a closed form formula based on a local approximation of  $g(\cdot, \mathbf{0})$ . Typically when  $\boldsymbol{\xi}_{\text{odo}}$  becomes larger than the attraction basin of the true minimum, the algorithm gets trapped by local minima and corresponding dispersion drastically jumps from a null value to a potentially large value. Given a magnitude  $\mathbf{Q}_{\text{odo}}$  of the odometry dispersion it is possible to “infer” a scale-dependent Jacobian  $\mathbf{J}$ , though, such that first order dispersion writes  $g(\boldsymbol{\xi}_{\text{odo}}, \mathbf{0}) \approx g(\mathbf{0}, \mathbf{0}) + \mathbf{J}\boldsymbol{\xi}_{\text{odo}}$  (in the present article we advocate the use of the unscented transform to compute  $\mathbf{J}$ , see Section III-B). Contrary to linearization w.r.t. sensor noise, each  $\mathbf{Q}_{\text{odo}}$  may yield a different  $\mathbf{J}$ . This yields a covariance  $\hat{\mathbf{Q}}_{\text{conv}}^{\text{wrong}} = \mathbf{J}\mathbf{Q}_{\text{odo}}\mathbf{J}^T$ . The linearized model corresponding to (5) finally writes:

$$\boldsymbol{\xi}_{\text{icp}} = g(\mathbf{0}, \mathbf{0}) + \mathbf{J}\boldsymbol{\xi}_{\text{odo}} + \mathbf{G}\mathbf{w}_{\text{sensor}}. \quad (6)$$

Recall the statistical results of Section II-A. The analogy is as follows. We have a first observation  $\mathbf{y}_1$  (odometry) and then a second  $\mathbf{y}_2$  (ICP) whose noise consists of two components. The second component  $\mathbf{G}\mathbf{w}_2$  is independent from other variables but the first  $\mathbf{J}\mathbf{w}_1$  is a function of odometry uncertainty: in the directions where we have a global minimum, odometry (i.e. initialization) uncertainty

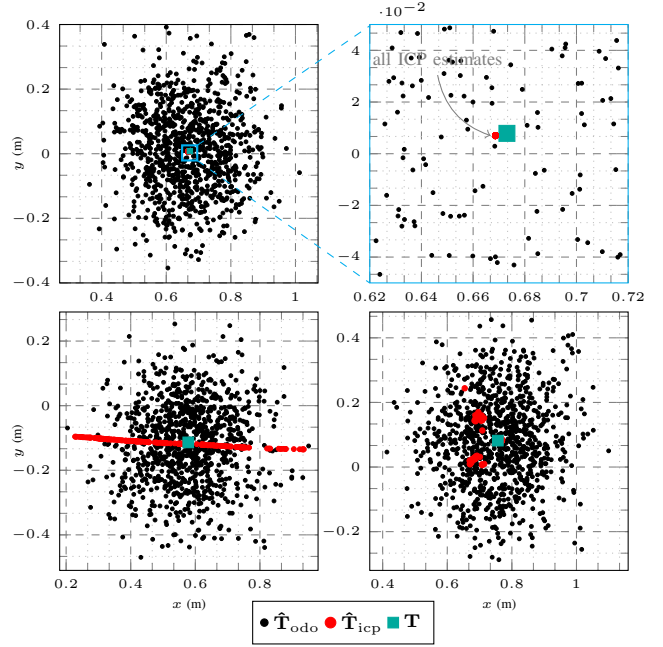


Fig. 3. ICP horizontal position initial estimates  $\hat{\mathbf{T}}_{\text{odo}}$ , ICP final estimates  $\hat{\mathbf{T}}_{\text{icp}}$  and ground-truth  $\mathbf{T}$  for registrations on the sequences *Apartment* (top), *Hauptgebaude* (bottom left) and *Gazebo summer* (bottom right) of [8], where we sample 1000 initial estimates. Formula (4) applies, where  $\mathbf{w}_{\text{sensor}}$  is fixed at the particular realizations where point clouds were recorded. Dispersion of black points are reflected by  $\mathbf{Q}_{\text{odo}}$  and of red points by  $\hat{\mathbf{Q}}_{\text{conv}}^{\text{wrong}}$ . Error of red points w.r.t. ground truth is encoded in  $\hat{\mathbf{Q}}_{\text{icp}} = \hat{\mathbf{Q}}_{\text{conv}}^{\text{wrong}} + \hat{\mathbf{Q}}_{\text{conv}}^{\text{at}}$ . Top left: example of global minimum,  $\hat{\mathbf{Q}}_{\text{conv}}^{\text{wrong}} = \mathbf{0}$  and there is no dispersion of red points. Top right (zoom): however there is a small error w.r.t. ground truth (since  $\mathbf{w}_{\text{sensor}} \neq \mathbf{0}$ ) whose magnitude is captured by  $\hat{\mathbf{Q}}_{\text{conv}}^{\text{at}}$ . Bottom left: underconstrained situation. In unobservable directions  $\mathbf{J}$  is the identity as the algorithm cannot improve initial estimate (whereas it is small along well observable directions). Corresponding dispersion (red points) at least at a large scale is thus the projection of initial dispersion on those directions. Bottom right: presence of local minima. Red points are scattered and regroup at local minima. Formula explains the situation as  $\hat{\mathbf{Q}}_{\text{icp}} = \hat{\mathbf{Q}}_{\text{conv}}^{\text{wrong}} + \hat{\mathbf{Q}}_{\text{conv}}^{\text{at}}$  and  $\hat{\mathbf{Q}}_{\text{conv}}^{\text{wrong}}$  reflects wrong convergence dispersion indeed.

has no effect, whereas in the directions where we have no information (e.g., corridor) ICP uncertainty is fully correlated with odometry's. Finally, in the directions where there are local minima ICP uncertainty writes as some factor (we may infer)  $\mathbf{J}$  times odometry noise. So we finally get our first main result relating uncertainties:

$$\hat{\mathbf{Q}}_{\text{icp}} = \hat{\mathbf{Q}}_{\text{conv}}^{\text{wrong}} + \hat{\mathbf{Q}}_{\text{conv}}^{\text{at}}. \quad (7)$$

with  $\hat{\mathbf{Q}}_{\text{conv}}^{\text{wrong}} = \mathbf{J}\mathbf{Q}_{\text{odo}}\mathbf{J}^T$  and  $\hat{\mathbf{Q}}_{\text{conv}}^{\text{at}} = \mathbf{G}\mathbf{Q}_{\text{sensor}}\mathbf{G}^T$ . Moreover, the covariance of the maximum likelihood estimate accounting for both ICP and odometry writes

$$\hat{\mathbf{Q}}_{\text{odo+icp}}^{-1} = \begin{bmatrix} \mathbf{1} \\ \mathbf{1} \end{bmatrix}^T \begin{bmatrix} \mathbf{Q}_{\text{odo}} & \mathbf{Q}_{\text{odo}}\mathbf{J}^T \\ \mathbf{J}\mathbf{Q}_{\text{odo}} & \hat{\mathbf{Q}}_{\text{conv}}^{\text{wrong}} + \hat{\mathbf{Q}}_{\text{conv}}^{\text{at}} \end{bmatrix}^{-1} \begin{bmatrix} \mathbf{1} \\ \mathbf{1} \end{bmatrix}. \quad (8)$$

**Remark 1.** It is important to distinguish between (7) that computes the statistical dispersion of ICP estimate  $\hat{\mathbf{T}}_{\text{icp}}$  stemming from sensor noise and initial uncertainty and (8) that reflects the information one has on the actual transformation  $\mathbf{T}$  in the light of both odometry and point clouds.

#### D. Experimental Evidence Using Real Data

To get insight into the obtained formulas, we first propose to consider the following simple cases:

1) *Case of Global Minimum:* no dispersion arises from initial dispersion, thus we have  $\mathbf{J} = \mathbf{0}$ . Information we have on the displacement combining sensors satisfies then  $\hat{\mathbf{Q}}_{\text{odo+icp}}^{-1} = \mathbf{Q}_{\text{odo}}^{-1} + (\hat{\mathbf{Q}}_{\text{conv}}^{\text{at}})^{-1}$  according to (8), which is logical. Moreover the dispersion is exclusively owed to sensor noise, leading to  $\hat{\mathbf{Q}}_{\text{icp}} = \hat{\mathbf{Q}}_{\text{conv}}^{\text{at}}$  from (7).

2) *Presence of Local Minima:* wrong convergence generates dispersion, and this tends to dominate the centimetric dispersion reflected by  $\hat{\mathbf{Q}}_{\text{conv}}^{\text{at}}$ .

3) *Underconstrained Situation:* the algorithm is “blind” in some directions which are impossible to observe, typically a corridor. In those directions  $\mathbf{J}$  will be the identity (the algorithm does not change initial estimate since in those directions its cost function is flat). On the contrary, unobservability is well captured locally, and closed form formulas (in theory) account for infinite eigenvalues of  $\hat{\mathbf{Q}}_{\text{conv}}^{\text{at}}$  in those directions. Then, applying (7) we see  $\hat{\mathbf{Q}}_{\text{icp}}$  is infinite in those directions indeed and cannot be trusted. However, in those directions the odometry should be solely trusted so it is logical that from (8) we see covariance of the best estimate equals odometry covariance (along unobservable directions).

To provide experimental evidence, inspired from the recent work [7] we focus on the role played by the ICP initialization value  $\hat{\mathbf{T}}_{\text{odo}}$ . Given real (fixed) point clouds  $\mathcal{P}$  and  $\mathcal{Q}$  (and thus fixed  $\mathbf{w}_{\text{sensor}}$ ), we massively sample  $\hat{\mathbf{T}}_{\text{odo}}$  from a coarse distribution around  $\mathbf{T}$  whose standard deviation has magnitude 0.2m and 10 deg, and compute ICP estimates, see Figure 3.

### III. COVARIANCE COMPUTATION

This section describes our algorithm for estimating the 3D ICP uncertainty covariance leveraging previous findings.

#### A. Computation of Small Dispersion owing to Noise

We compute  $\hat{\mathbf{Q}}_{\text{conv}}^{\text{at}}$  by inserting an *unknown* bias error on each point measurement and following then the closed form methodology of [6,17]. Assuming the ICP converges to the true minimum, the estimated rotation matrix  $\hat{\mathbf{R}}_{\text{icp}} \in SO(3)$  and translation  $\hat{\mathbf{t}}_{\text{icp}} \in \mathbb{R}^3$  that compose  $\hat{\mathbf{T}}_{\text{icp}}$  are obtained as

$$\hat{\mathbf{R}}_{\text{icp}}, \hat{\mathbf{t}}_{\text{icp}} = \arg \min_{\mathbf{R}, \mathbf{t}} \sum_k \|w_k \mathbf{n}_k^T (\mathbf{R} \hat{\mathbf{p}}_k + \mathbf{t} - \hat{\mathbf{q}}_k)\|_2^2, \quad (9)$$

where  $\hat{\mathbf{p}}_k \in \mathbb{R}^3$  is the measured  $k$ -th point in  $\mathcal{P}$  and  $\hat{\mathbf{q}}_k \in \mathbb{R}^3$  its associated point in  $\mathcal{Q}$ , and  $w_k$  a scalar weight for considering robust filtering and depth sensor noise [5]. The vector  $\mathbf{n}_k \in \mathbb{R}^3$  represents the normal at  $\hat{\mathbf{p}}_k$ , as we consider the point-to-plane error metric recommended in [17].

Linearizing the ICP objective  $J(\cdot)$  given in the right part of (9) at  $\hat{\mathbf{R}}_{\text{icp}}, \hat{\mathbf{t}}_{\text{icp}}$ , i.e. at  $\hat{\mathbf{T}}_{\text{icp}}$ , we get the cost  $J_{\hat{\mathbf{T}}_{\text{icp}}}(\cdot)$  as

$$J_{\hat{\mathbf{T}}_{\text{icp}}}(\boldsymbol{\xi}) := J\left(\exp(\boldsymbol{\xi}) \hat{\mathbf{T}}_{\text{icp}}\right) \quad (10)$$

$$\approx \sum_k \|\mathbf{B}_k \boldsymbol{\xi} + \mathbf{C}_k \mathbf{w} + d_k\|_2^2, \quad (11)$$

---

#### Algorithm 1: proposed computation of $\hat{\mathbf{Q}}_{\text{conv}}^{\text{wrong}}, \hat{\mathbf{Q}}_{\text{cross}}$

---

**Input:**  $\mathcal{P}, \mathcal{Q}, \hat{\mathbf{T}}_{\text{odo}}, \mathbf{Q}_{\text{odo}}, \hat{\mathbf{T}}_{\text{icp}}$ ;  
 // set sigma points  
 1  $\boldsymbol{\xi}_{\text{odo}}^j = \text{col}(\sqrt{6\mathbf{Q}_{\text{odo}}})_j, j = 1, \dots, 6,$   
 $\boldsymbol{\xi}_{\text{odo}}^j = -\text{col}(\sqrt{6\mathbf{Q}_{\text{odo}}})_{j-6}, j = 7, \dots, 12;$   
 // propagate sigma points through ICP  
 2  $\hat{\mathbf{T}}_{\text{icp}}^j = \text{icp}(\mathcal{P}, \mathcal{Q}, \exp(\boldsymbol{\xi}_{\text{odo}}^j) \hat{\mathbf{T}}_{\text{odo}}), j = 1, \dots, 12;$   
 3  $\hat{\boldsymbol{\xi}}_{\text{icp}}^j = \log(\hat{\mathbf{T}}_{\text{icp}}^j \hat{\mathbf{T}}_{\text{icp}}^{-1}), j = 1, \dots, 12;$   
 // compute covariance  
 4  $\hat{\mathbf{Q}}_{\text{conv}}^{\text{wrong}} = \sum_{j=1}^{12} \frac{1}{12} \hat{\boldsymbol{\xi}}_{\text{icp}}^j \hat{\boldsymbol{\xi}}_{\text{icp}}^{jT};$   
 // infer cross-covariance  
 5  $\hat{\boldsymbol{\xi}}_{\text{icp}} = \sum_{j=1}^{12} \frac{1}{12} \hat{\boldsymbol{\xi}}_{\text{icp}}^j;$   
 6  $\hat{\mathbf{Q}}_{\text{cross}} = \sum_{j=1}^{12} \frac{1}{12} \boldsymbol{\xi}_{\text{odo}}^j (\hat{\boldsymbol{\xi}}_{\text{icp}}^j - \hat{\boldsymbol{\xi}}_{\text{icp}})^T;$   
**Output:**  $\hat{\mathbf{Q}}_{\text{conv}}^{\text{wrong}}, \hat{\mathbf{Q}}_{\text{cross}};$

---

where  $\boldsymbol{\xi} \sim \mathcal{N}(\mathbf{0}, \hat{\mathbf{Q}}_{\text{conv}}^{\text{at}})$  corresponds to the ICP uncertainty at small scale,  $\mathbf{w} \in \mathbb{R}^l$  is the *unknown* bias of dimension  $l$ ,  $\mathbf{B}_k \in \mathbb{R}^{1 \times 6}$  and  $\mathbf{C}_k \in \mathbb{R}^{1 \times l}$  are matrices, and  $d_k = w_k \mathbf{n}_k^T (\hat{\mathbf{R}} \hat{\mathbf{p}}_k + \hat{\mathbf{t}} - \hat{\mathbf{q}}_k)$  a scalar. Following least squares covariance [6,17], we compute the covariance of  $\boldsymbol{\xi}$  as

$$\hat{\mathbf{Q}}_{\text{conv}}^{\text{at}} = \mathbf{A}^{-1} + \mathbf{A}^{-1} \mathbf{B} \text{cov}(\mathbf{w}) \mathbf{B}^T \mathbf{A}^{-1}, \quad (12)$$

where  $\mathbf{A} = \sum_k \mathbf{B}_k^T \mathbf{B}_k$ , and  $\mathbf{B} = \sum_k \mathbf{B}_k \mathbf{C}_k^T$ . We recover the covariance  $\mathbf{A}^{-1}$  of [6,17] w.r.t. sensor white noise, and a new term,  $\mathbf{A}^{-1} \mathbf{B} \text{cov}(\mathbf{w}) \mathbf{B}^T \mathbf{A}^{-1}$ , that represents the covariance w.r.t. the unknown bias  $\mathbf{w}$ , that is, correlated noise. This new additional term is paramount as  $\mathbf{A}$  has magnitude proportional to the number of points in the cloud hence  $\mathbf{A}^{-1}$  is very small, typically less than millimeter, explaining that Censi’s formula (based on  $\mathbf{A}^{-1}$  only) seems overoptimistic [20]. According to the law of statistics if the noise were white multiplying the number of points by 2 would lead in a factor 2 variance decrease but we see in practice there’s a lower bound on ICP accuracy (typically nanometer accuracy is beyond reach no matter how many points in the cloud) owing to the presence of a bias  $\mathbf{w}$  arising from calibration, temperature drift, laser stability [13], observed material [5], and incidence of beams [14]. We assume the bias to be unknown with  $\text{cov}(\mathbf{w}) = \sigma^2 \mathbf{I}$ , where  $\sigma$  is the standard deviation of the depth bias, whose value is typically close to 5cm in [5]. Derivation of  $\mathbf{B}_k$  and  $\mathbf{C}_k$  is provided in Appendix.

#### B. Computation of Dispersion owing to Wrong Convergence

Computation of  $\hat{\mathbf{Q}}_{\text{conv}}^{\text{wrong}}$  is of greater importance as in practice it largely dominates  $\hat{\mathbf{Q}}_{\text{conv}}^{\text{at}}$ . We propose to compute it in a deterministic derivative-free method, in which we adapt the unscented transform [21] for the pose  $\mathbf{T} \in SE(3)$  by following [22,26]. The advantages of using our unscented based method rather than Monte-Carlo sampling are fourfold: 1) it is deterministic; 2) it keeps computationally reasonable by adding only 12 ICP registrations which are easily parallelisable; 3) it explicitly computes the cross-covariance

matrix between  $\hat{\mathbf{T}}_{\text{icp}}$  and  $\hat{\mathbf{T}}_{\text{odo}}$  as a by-product without extra computational operations; and 4) it scales with  $\mathbf{Q}_{\text{odo}}$ , i.e. our approach naturally self-adapts to the confidence we have in odometry without extra parameter tuning.

We compute  $\hat{\mathbf{Q}}_{\text{conv}}^{\text{wrong}}$  as follows, see Algorithm 1:

- we consider the prior distribution  $\mathbf{T}_{\text{prior}} \sim \mathcal{N}_R(\hat{\mathbf{T}}_{\text{odo}}, \mathbf{Q}_{\text{odo}})$ , which is approximated by a set of so-called sigma-points  $\xi_{\text{odo}}^j$ , see step 1);
- we approximate the propagated distribution  $\mathbf{T}_{\text{prop}} = \text{icp}(\mathcal{P}, \mathcal{Q}, \mathbf{T}_{\text{prior}})$  as

$$\mathbf{T}_{\text{prop}} = \text{icp}\left(\mathcal{P}, \mathcal{Q}, \mathcal{N}_R\left(\hat{\mathbf{T}}_{\text{odo}}, \mathbf{Q}_{\text{odo}}\right)\right) \quad (13)$$

$$\sim \mathcal{N}_R\left(\hat{\mathbf{T}}_{\text{icp}}, \hat{\mathbf{Q}}_{\text{conv}}^{\text{wrong}}\right), \quad (14)$$

after propagating each sigma-point in steps 2) and 3), where  $\hat{\mathbf{T}}_{\text{icp}}$  is the given ICP estimate, that requires the computations of 12 additional registrations whereas the rest of the algorithm is computationally negligible. We compute  $\hat{\mathbf{Q}}_{\text{conv}}^{\text{wrong}}$  and infer the cross-covariance  $\hat{\mathbf{Q}}_{\text{cross}} = \mathbf{J}\mathbf{Q}_{\text{odo}}$  between propagated and prior distributions as a by-product in respectively steps 4) and 6).

We derive the algorithm by following [22] for pose measurement, zero-mean prior distribution, and where we set  $\alpha = 1$ . Note that estimate  $\hat{\xi}_{\text{icp}}$  computed in step 5) allows correcting or rejecting ICP registration failure, albeit beyond the scope of the present paper concerned with ICP estimate uncertainty assessment. We finally indicate that this part of the method is highly versatile as independent to the chosen metric: considering a different metric, see [4], requires no modification.

## IV. EXPERIMENTAL RESULTS

### A. Dataset Description & ICP Algorithm Setting

This section evaluates the ability of the approach to estimate ICP uncertainty on the *Challenging data sets for point cloud registration algorithms* [8]. It comprises eight sequences where point clouds are taken in environments ranging from structured to unstructured, and indoor to outdoor. Each sequence contains between 31 and 45 point cloud scans along with ground-truth pose for each scan, that provides a total of 268 different registrations as we register scans acquired successively.

We configure the ICP as in [9] with 95% random subsampling, kd-tree for data association, and point-to-plane error metric where we keep the 70% closest point associations for rejecting outlier.

### B. Compared Methods and Evaluation Metrics

This section evaluates the following methods:

$\hat{\mathbf{Q}}_{\text{censi}}$  : the close-form method of [6] adapted for the ICP point-to-plane metric defined in (9);

$\hat{\mathbf{Q}}_{\text{carlo}}^{\text{monte}}$  : the covariance computed after sampling of 65 Monte-Carlo ICP estimates, which is more than five times the execution time of the proposed approach;

$\hat{\mathbf{Q}}_{\text{icp}}$  : our proposed approach detailed in Section III.

Each method assumes depth sensor white noise and bias with 5 cm standard deviation, which is the mean value found in

metric	NNE		KL div.	
	trans.	rot.	trans.	rot.
$\hat{\mathbf{Q}}_{\text{censi}}$	22	$10^2$	$10^3$	$10^5$
$\hat{\mathbf{Q}}_{\text{carlo}}^{\text{monte}}$	3.6	15	$10^3$	$10^3$
$\hat{\mathbf{Q}}_{\text{icp}}$ (proposed)	<b>0.6</b>	<b>3.7</b>	<b>46</b>	<b><math>10^2</math></b>

Table 1. Results of ICP uncertainty estimation in term of Normalized Norm Error (NNE) and Kullback-Leibler divergence (KL div.) divided into translation and rotation parts, and averaged over the eight sequences of [8]. The proposed method outperforms the two others.

[5] for the Hokuyo sensor used for these experiments, and all methods know the initial uncertainty  $\mathbf{Q}_{\text{odo}}$ , whose magnitude 0.2 m and 10 deg corresponds to the easy scenario of [9].

We compare the above methods using two metrics:

1) *Normalized Norm Error (NNE)*: that evaluates the historically challenging [6,16] prediction of the covariance scale, and is computed as

$$\text{NNE} = \left(\frac{1}{N} \sum_{n=1}^N \|\xi_n\|_2^2 / \text{trace}(\hat{\mathbf{Q}}_n)\right)^{1/2}, \quad (15)$$

where  $\xi_n = \log(\hat{\mathbf{T}}_n \mathbf{T}^{-1})$  is the transformation error and  $\hat{\mathbf{Q}}_n$  the estimated uncertainty covariance matrix, and averaged over  $N$  samples. This metrics characterizes the uncertainty as only the true registration is known (the exact distribution of the point cloud is unknown). The target value is one, below one the estimation is pessimist, whereas a value over one indicates an overoptimistic estimation.

2) *Kullback-Leibler Divergence (KL div.)*: which is computed between a pseudo-true distribution and the estimated distribution. The pseudo-true distribution is computed after sampling 1000 ICP estimates of the evaluated registration over the initial position. As sensor noise is fixed in the point clouds, this distribution represents the uncertainty coming from poor initialization and evaluates the shape of the covariance estimates.

### C. Results

Results are averaged over 1000 initializations for each of the 268 considered pairs of point clouds, representing a total of 260 000 registrations, where the ICP is initialized with a different estimate  $\hat{\mathbf{T}}_{\text{odo}}$  sampled from  $\mathcal{N}_R(\mathbf{T}, \mathbf{Q}_{\text{odo}})$ . As the ICP error distributions are not Gaussian [9], we make our statistic more robust by removing both the more and less accurate quantiles of each registration. Table 1 provides average results, and Figure 4 illustrates typical registrations from structured to unstructured environments. We observe:

- $\hat{\mathbf{Q}}_{\text{censi}}$  is far too optimistic and unreliable for sensor-fusion, as noted in [20]. Its centimetric confidence interval makes sense only when ICP is very accurate;
- $\hat{\mathbf{Q}}_{\text{carlo}}^{\text{monte}}$  is overoptimistic when the discrepancy arising from ICP initialization remains negligible, see Figure 4 (top and bottom left), for which the method predicts a confidence interval with millimetric size. This is naturally explained as the method assumes no error caused by sensor noises;

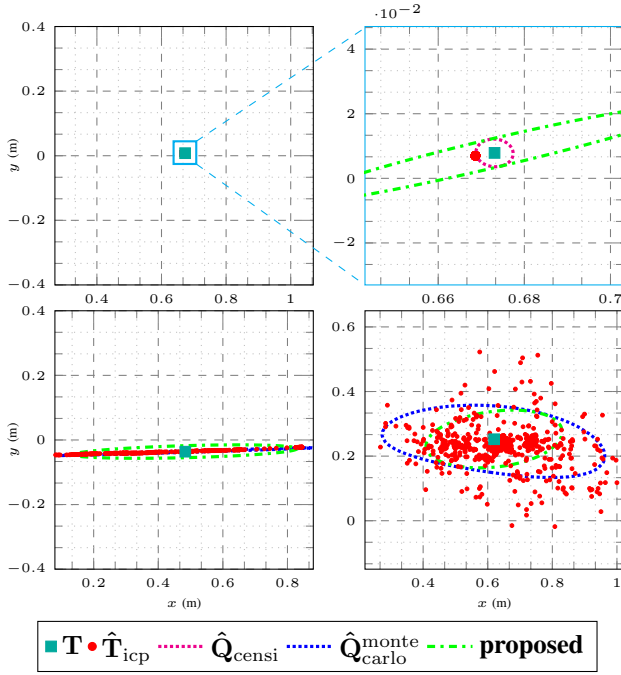


Fig. 4. Results on real data of [8] projected on the ground plane for visualization. Ellipses represent the 95% ( $3\sigma$ ) confidence sets for each uncertainty estimation method. Top left, *Apartment*: “true convergence situation”, the errors are mainly caused by sensor noises and Censi’s formula should apply. Top right: zoom, however we see the red dotted ellipse (Censi) seems optimistic as ground truth is almost outside it whereas it falls well within our ellipse (green dashed). Bottom left, *Hauptgebäude*; bottom right, *Mountain*: “wrong convergence”, the large errors are due ICP initialization. Only our approach is consistent with ICP uncertainty in each environment and does not suffer from overoptimism.

- the proposed method obtains the best results for both metrics as displayed in Table 1. It notably outperforms  $\hat{Q}_{\text{carlo}}^{\text{monte}}$  while deterministic hence more reliable, and computationally much cheaper. We note the sensor bias consideration using for computing  $\hat{Q}_{\text{conv}}^{\text{at}}$  slightly inflates the covariance computed through [6], which more closely reflects actual uncertainty in specific “true convergence” cases, see Figure 4 (top), although the dominant term is  $\hat{Q}_{\text{conv}}^{\text{wrong}}$  in general.

Besides outperforming the other methods, our method provides simple parameter tuning: we set the bias noise standard deviation as having same magnitude as sensor white noise, and the error stemming from ICP initialization does not need to be tuned since  $\mathbf{Q}_{\text{odo}}$  is an output of inertial, visual, or wheeled odometry system [2,3].

## V. APPLICATION TO POSE-GRAPH LOCALIZATION

A pose-graph is a special case of a factor-graph where all the variables being estimated are robot poses along the robot trajectory [30], and the factors between these poses are relative pose measurements. Each factor  $\mathcal{N}_R(\hat{\mathbf{T}}, \hat{\mathbf{Q}})$  is parameterized by a measurement  $\hat{\mathbf{T}}$  and a covariance matrix  $\hat{\mathbf{Q}}$  (or equivalently with the inverse of the ICP covariance matrix, a.k.a. information matrix) that assesses confidence in the measurement. Our goal in this section is to combine odometry with ICP relative transformations through pose

graph optimization for robot localization, and to show that ICP and odometry sensors are complementary as odometry may prevent ICP failures. We also demonstrate that correctly assessing ICP uncertainty improves accuracy, robustness and consistency of estimations.

### A. Compared Methods and Evaluation Metrics

We compare on the sequences of [8] different pose-graphs defined as follow:

- odo. : based on pure odometry factors  $\mathcal{N}_R(\hat{\mathbf{T}}_{\text{odo}}, \mathbf{Q}_{\text{odo}})$ ;
- CELLO-3D : reproduced results of [7], that proposes a learning based method for estimating the ICP covariance, which is trained on environments similar to the tested sequence. The results are indicative as the ICP setting of [7] slightly differs from the setting of [9] we use;
- odo.+ICP : combines odometry  $\mathcal{N}_R(\hat{\mathbf{T}}_{\text{odo}}, \mathbf{Q}_{\text{odo}})$  and ICP  $\mathcal{N}_R(\hat{\mathbf{T}}_{\text{icp}}, \hat{\mathbf{Q}}_{\text{icp}})$  measurements with our proposed covariance estimates considering them as independent measurements, as in Figure 2 (left) and e.g. [2];
- proposed** : involves odometry  $\mathcal{N}_R(\hat{\mathbf{T}}_{\text{odo}}, \mathbf{Q}_{\text{odo}})$  and ICP  $\mathcal{N}_R(\hat{\mathbf{T}}_{\text{icp}}, \hat{\mathbf{Q}}_{\text{icp}})$  estimates along with the cross-correlation term  $\hat{\mathbf{Q}}_{\text{cross}}$ , see Figure 2 (right). Based on Section II, we prune ICP registration from the pose-graph using a Neyman-Pearson statistical test about difference between the ICP and odometry  $\log(\hat{\mathbf{T}}_{\text{icp}}^{-1}\hat{\mathbf{T}}_{\text{odo}})$ .

We set odometry errors with standard deviation magnitudes 0.15 m and 4 deg. We compute the pose-graph based on [26] through: 1) the fusion of the odometry and ICP estimates; and 2) the compound of the covariances at two successive scans with a closed-form expression from [26]. This novel fusion scheme of two *correlated* poses is an independent contribution, whose implementation is available online.

We evaluate the above methods using two metrics:

- 1) *Mahalanobis Distance (Mah. dist.)*: between the final trajectory estimates and the ground truth

$$\text{Mah. dist.} = \left( \sum_{n=0}^N \frac{\xi_n^T \hat{\mathbf{Q}}_n^{-1} \xi_n}{\dim(\xi_n)N} \right)^{1/2}, \quad (16)$$

where  $\xi_n = \log(\hat{\mathbf{T}}_n \mathbf{T}^{-1})$  is the true transformation error and  $\hat{\mathbf{Q}}_n$  the estimated uncertainty covariance matrix, and averaged over  $N$  samples. As NNE, the target value is one, below one the estimation is pessimistic, whereas a value over one indicates optimistic estimate.

- 2) *Root Mean Square Error (RMSE)*: which averages the final pose error along each sequence trajectory and reveals the accuracy of a given method.

### B. Pose-Graph Localization Results

We average results over 40 different odometry trajectories for each sequence, i.e. for a total of 160 sequences. Table 2 and Table 3 display numerical results for each metric and illustrations from indoor to outdoor environments are shown in Figure 5. We observe:

- the odometry estimation drifts and becomes hardly informative at the end of each trajectory; hence its RMSE is high;

sequence	Apartment		Hauptgebaude		Stairs		Mountain		Gazebo summer		Gazebo winter		Wood summer		Wood winter	
Mah. dist.	trans.	rot.	trans.	rot.	trans.	rot.	trans.	rot.	trans.	rot.	trans.	rot.	trans.	rot.	trans.	rot.
CELLO-3D [7]	0.2	<b>0.1</b>	0.3	0.2	0.1	0.2	-	-	0.2	0.2	0.1	0.2	0.1	<b>0.3</b>	0.1	<b>0.3</b>
odo.+ICP	3.5	15	1.9	3.2	<b>1.1</b>	<b>4.2</b>	1.5	<b>1.2</b>	1.1	<b>2.1</b>	1.9	<b>3.7</b>	<b>1.5</b>	4.6	<b>1.2</b>	4.8
<b>proposed</b>	<b>2.3</b>	<b>9.8</b>	<b>1.8</b>	<b>2.9</b>	<b>1.1</b>	<b>4.2</b>	<b>1.2</b>	<b>1.2</b>	<b>1.0</b>	2.3	<b>1.8</b>	<b>3.7</b>	<b>1.5</b>	4.7	<b>1.2</b>	4.2

Table 2. Pose-graph **consistency results in term of Mahalanobis distance** split into translation and rotation parts for the eight sequences of [8], where *Mountain* is not considered in [7]. Odometry only computed using close-form expressions of [26] achieves close to 1 metric and is not shown since it does not involve ICP. Our method obtains on average the best uncertainty assessment, albeit slightly optimistic.

sequence	Apartment		Hauptgebaude		Stairs		Mountain		Gazebo summer		Gazebo winter		Wood summer		Wood winter	
RMSE	trans.	rot.	trans.	rot.	trans.	rot.	trans.	rot.	trans.	rot.	trans.	rot.	trans.	rot.	trans.	rot.
odo.	0.9	15	2.4	12	1.1	12	2.0	10	0.8	13	0.9	13	2.3	14	1.6	12
odo.+ICP	0.4	8.0	<b>0.5</b>	1.6	<b>0.4</b>	<b>4.5</b>	<b>0.9</b>	4.3	0.1	1.5	<b>0.1</b>	<b>0.8</b>	<b>0.2</b>	<b>1.3</b>	<b>0.1</b>	0.7
<b>proposed</b>	<b>0.3</b>	<b>5.8</b>	<b>0.5</b>	<b>1.5</b>	<b>0.4</b>	<b>4.5</b>	<b>0.9</b>	<b>3.9</b>	<b>0.1</b>	<b>1.3</b>	<b>0.1</b>	<b>0.8</b>	<b>0.2</b>	<b>1.3</b>	<b>0.1</b>	<b>0.6</b>

Table 3. Pose-graph **accuracy results in term of root mean square error RMSE** split into translation and rotation (in m and deg) for the eight sequences of [8]. Correctly assessing covariance correlation slightly improves as a byproduct of better uncertainty assessment.

- odo.+ICP is subject to registration failures, see Figure 5 (top chart). Albeit locally consistent, these strong failures highly degrade both metrics, particularly in the sequence *Apartment*;
- CELLO-3D is the only pessimistic method, which estimates uncertainty ranging from 3 to 10 times higher than actual uncertainty. It evidences how difficult it is to assess ICP covariance;
- the proposed approach obtains in average the best results, regarding both accuracy and consistency. It obtains similar estimates than odo.+ICP when the ICP algorithm is accurate as in Figure 5 (bottom). However, in some scenarios it better incorporates odometry than odo.+ICP thanks to its accounting for measurement correlation, see Figure 5 (middle). It even manages to reject some ICP registration failures thanks to our simple and slightly conservative outliers rejection threshold. However, some ICP failures keep undetected, explaining thus the high metrics, particularly for orientation, of the sequence *Apartment*.

Preventing such ICP failures is difficult and constitutes a full research topic, see e.g. [31], which is beyond the scope of the present paper. Future work will address this problem by leveraging the approach and the discrepancy in the propagated sigma points computed in Section III-B. As in Section IV, the algorithm better captures translation than rotation uncertainty.

## VI. CONCLUSION

This paper presents a novel method for real time estimation of 3D uncertainty covariance matrix of the ICP algorithm. The method relies on a careful study of the influence of both sensor noises and algorithm initialization on the ICP estimates, that we leverage in a deterministic scheme which remains very simple in terms of parameter tuning. The core of our approach is versatile as not restricted to an ICP configuration, such that one can apply it to any choice of error metrics and ICP setting with no modification. The approach is successfully validated on individual pairs of point clouds and over trajectories on challenging real datasets, where it obtains consistent results that correctly reflect sampled trajec-

tories. We also apply the method to pose-graph localization, and show it outperforms other fusion methods in terms of accuracy, robustness and consistency of the estimates along the full trajectory.

Future work will address the benefit of the method for preventing ICP failures, particularly its coupling with learning-based methods, and for fusing odometry, ICP and GNSS in Kalman filtering and optimization-based schemes.

## APPENDIX

We detail the computation of matrices  $\mathbf{B}_k$  and  $\mathbf{C}_k$  in (9). We define depth bias for each point cloud  $\mathcal{P}$  and  $\mathcal{Q}$ , and further assume for simplicity that each frame is centered on the laser sensor. Thus, each pair  $(\mathbf{p}_k, \mathbf{q}_k)$  of true points is measured as

$$\begin{bmatrix} \mathbf{p}_k \\ \mathbf{q}_k \end{bmatrix} = \begin{bmatrix} \hat{\mathbf{p}}_k \\ \hat{\mathbf{q}}_k \end{bmatrix} + \begin{bmatrix} \frac{\hat{\mathbf{p}}_k}{\|\hat{\mathbf{p}}_k\|_2} & \mathbf{0} \\ \mathbf{0} & \frac{\hat{\mathbf{q}}_k}{\|\hat{\mathbf{q}}_k\|_2} \end{bmatrix} \mathbf{w}, \quad (17)$$

where  $\hat{\mathbf{p}}_k/\|\hat{\mathbf{p}}_k\|_2$  and  $\hat{\mathbf{q}}_k/\|\hat{\mathbf{q}}_k\|_2$  correspond respectively to the direction to the points  $\mathbf{p}_k$  and  $\mathbf{q}_k$ . Linearising then the ICP registration error as  $\exp(\boldsymbol{\xi}) \hat{\mathbf{T}}_{\text{ICP}} \approx (\mathbf{I} + (\boldsymbol{\xi})_{SE(3)}^\wedge) \hat{\mathbf{T}}_{\text{ICP}}$  and plugging it into (11), leads to

$$\mathbf{B}_k = w_k \mathbf{n}_k^T \left[ - \left( \hat{\mathbf{R}} \hat{\mathbf{p}}_k + \hat{\mathbf{t}} \right)_{SO(3)}^\wedge \quad \mathbf{I} \right] \quad (18)$$

$$\mathbf{C}_k = w_k \mathbf{n}_k^T \left[ \frac{\hat{\mathbf{p}}_k}{\|\hat{\mathbf{p}}_k\|_2} \quad - \frac{\hat{\mathbf{q}}_k}{\|\hat{\mathbf{q}}_k\|_2} \right], \quad (19)$$

where  $(\cdot)_{SE(3)}^\wedge$  and  $(\cdot)_{SO(3)}^\wedge$  are respectively the overloaded wedge operators as defined for  $SE(3)$  and  $SO(3)$  in [26], where  $(\cdot)_{SO(3)}^\wedge$  is also known as the skew symmetric operator.

## REFERENCES

- [1] F. Pomerleau, F. Colas, and R. Siegwart, “A Review of Point Cloud Registration Algorithms for Mobile Robotics,” *Foundations and Trends in Robotics*, vol. 4, no. 1, pp. 1–104, 2015.
- [2] R. Dube, A. Gawel, H. Sommer, J. Nieto, R. Siegwart, and C. Cadena, “An Online Multi-robot SLAM System for 3D LiDARs,” in *International Conference on Intelligent Robots and Systems (IROS)*. IEEE, 2017, pp. 1004–1011.
- [3] P. Geneva, K. Eickenhoff, Y. Yang, and G. Huang, “LIPS: LiDAR-Inertial 3D Plane SLAM,” in *International Conference on Intelligent Robots and Systems (IROS)*. IEEE, 2018, pp. 123–130.

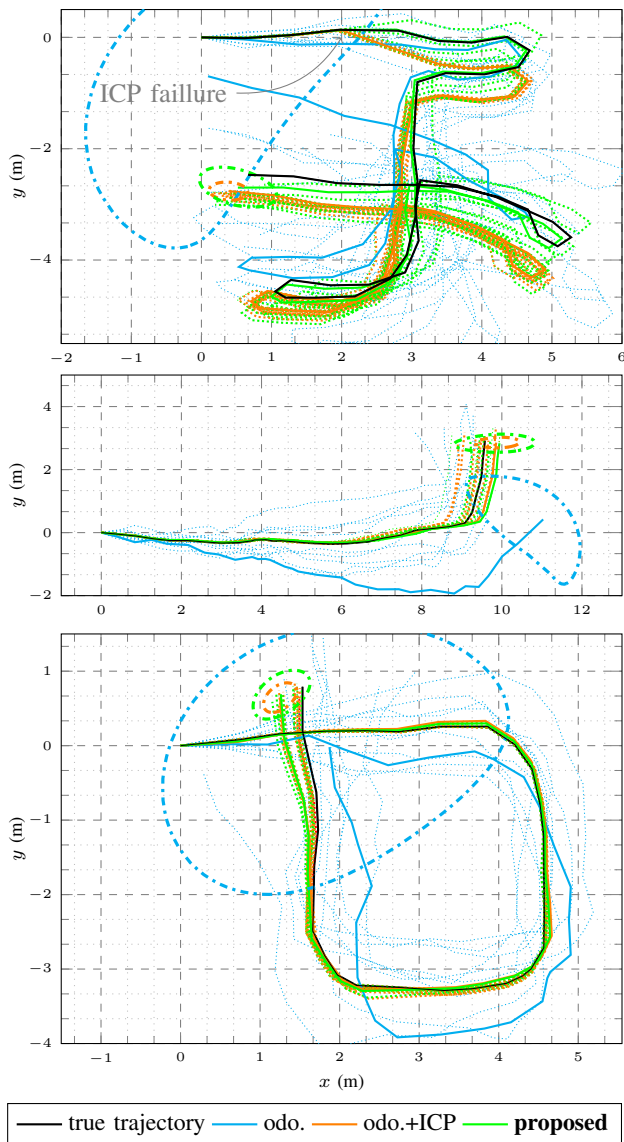


Fig. 5. Results in the *Apartment* (top), *Stairs* (middle) and *Gazebo summer* (bottom) sequences of [8], where the ICP algorithm gets respectively some failure registrations, moderately accurate estimates, and fully accurate estimates. Results are projected on the ground plane for visualization where the “ellipses” represent the 95% ( $3\sigma$ ) final confidence sets. The definition of the uncertainty in the Lie algebra of  $SE(3)$  in (3) explains the shapes of the “ellipses”, see e.g. [22,26]. The proposed method obtains more accurate (proximity to ground truth) and consistent (discrepancy w.r.t. ground truth well represented by the ellipse) results than the other methods.

[4] P. Babin, P. Giguère, and F. Pomerleau, “Analysis of Robust Functions for Registration Algorithms,” in *International Conference on Robotics and Automation (ICRA)*. IEEE, 2019.

[5] F. Pomerleau, A. Breitenmoser, M. Liu, F. Colas, and R. Siegwart, “Noise Characterization of Depth Sensors for Surface Inspections,” in *International Conference on Applied Robotics for the Power Industry (CARPI)*. IEEE, 2012, pp. 16–21.

[6] A. Censi, “An Accurate Closed-form Estimate of ICP’s Covariance,” in *International Conference on Robotics and Automation (ICRA)*. IEEE, 2007, pp. 3167–3172.

[7] D. Landry, F. Pomerleau, and P. Giguère, “CELLO-3D: Estimating the Covariance of ICP in the Real World,” in *International Conference on Robotics and Automation (ICRA)*, 2019.

[8] F. Pomerleau, M. Liu, F. Colas, and R. Siegwart, “Challenging Data Sets for Point Cloud Registration Algorithms,” *The International*

*Journal of Robotics Research*, vol. 31, no. 14, pp. 1705–1711, 2012.

[9] F. Pomerleau, F. Colas, R. Siegwart, and S. Magnenat, “Comparing ICP Variants on Real-world Data Sets: Open-source Library and Experimental Protocol,” *Auton. Robots*, vol. 34, no. 3, pp. 133–148, 2013.

[10] M. Barczyk, S. Bonnabel, J.-E. Deschaud, and F. Goulette, “Invariant EKF Design for Scan Matching-Aided Localization,” *IEEE Trans. Contr. Syst. Technol.*, vol. 23, no. 6, pp. 2440–2448, 2015.

[11] M. Barczyk and S. Bonnabel, “Towards Realistic Covariance Estimation of ICP-based Kinect V1 Scan Matching: The 1D Case,” in *American Control Conference (ACC)*. IEEE, 2017, pp. 4833–4838.

[12] T. M. Iversen, A. G. Buch, and D. Kraft, “Prediction of ICP Pose Uncertainties Using Monte Carlo Simulation with Synthetic Depth Images,” in *International Conference on Intelligent Robots and Systems (IROS)*. IEEE, 2017, pp. 4640–4647.

[13] Z. Wang, Y. Liu, Q. Liao, H. Ye, M. Liu, and L. Wang, “Characterization of a RS-LiDAR for 3D Perception,” in *International Conference on Technology in Automation, Control, and Intelligent Systems (CYBER)*, 2018.

[14] J. Laconte, S.-P. Deschênes, M. Labussière, and F. Pomerleau, “LiDAR Measurement Bias Estimation via Return Waveform Modelling in a Context of 3D Mapping,” in *International Conference on Robotics and Automation (ICRA)*, 2019.

[15] J.-E. Deschaud, “IMLS-SLAM: Scan-to-Model Matching Based on 3D Data,” in *International Conference on Robotics and Automation (ICRA)*. IEEE, 2018, pp. 2480–2485.

[16] O. Bengtsson and A.-J. Baereldt, “Robot Localization Based on Scan-matching,” *Robotics and Autonomous Systems*, vol. 44, no. 1, pp. 29–40, 2003.

[17] S. Bonnabel, M. Barczyk, and F. Goulette, “On the Covariance of ICP-based Scan-matching Techniques,” in *American Control Conference (ACC)*. IEEE, 2016, pp. 5498–5503.

[18] S. M. Prakhya, L. Bingbing, Y. Rui, and W. Lin, “A Closed-form Estimate of 3D ICP Covariance,” in *International Conference on Machine Vision Applications*. IEEE, 2015, pp. 526–529.

[19] A. Shetty and G. Xingxin Gao, “Adaptive Covariance Estimation of LiDAR-based Positioning Errors for UAVs,” *Navigation*, vol. 66, no. 2, pp. 463–476, 2019.

[20] E. Mendes, P. Koch, and S. Lacroix, “ICP-based Pose-graph SLAM,” in *International Symposium on Safety, Security, and Rescue Robotics (SSRR)*. IEEE, 2016, pp. 195–200.

[21] S. Julier, J. Uhlmann, and H. Durrant-Whyte, “A New Method for the Nonlinear Transformation of Means and Covariances in Filters and Estimators,” *IEEE trans. automat. contr.*, vol. 45, no. 3, pp. 477–482, 2000.

[22] M. Brossard, S. Bonnabel, and J.-P. Condomines, “Unscented Kalman filtering on Lie groups,” in *International Conference on Intelligent Robots and Systems (IROS)*. IEEE, 2017, pp. 2485–2491.

[23] F. Dellaert, “Factor Graphs and GTSAM: A Hands-on Introduction,” *Technical Report GT-RIM-CP&R-2012-002*, Georgia Institute of Technology, 2012.

[24] R. Kummerle, G. Grisetti, H. Strasdat, K. Konolige, and W. Burgard, “G2o: A General Framework for Graph Optimization,” in *International Conference on Robotics and Automation (ICRA)*. IEEE, 2011, pp. 3607–3613.

[25] A. Barrau and S. Bonnabel, “Invariant Kalman Filtering,” *Annual Review of Control, Robotics, and Autonomous Systems*, vol. 1, no. 1, pp. 237–257, 2018.

[26] T. Barfoot and P. Furgale, “Associating Uncertainty With Three-Dimensional Poses for Use in Estimation Problems,” *IEEE trans. robot.*, vol. 30, no. 3, pp. 679–693, 2014.

[27] A. Barrau and S. Bonnabel, “The Invariant Extended Kalman Filter as a Stable Observer,” *IEEE trans. automat. contr.*, vol. 62, no. 4, pp. 1797–1812, 2017.

[28] G. Bourmaud, R. Mégret, M. Arnaudon, and A. Giremus, “Continuous-Discrete Extended Kalman Filter on Matrix Lie Groups Using Concentrated Gaussian Distributions,” *Journal of Mathematical Imaging and Vision*, vol. 51, no. 1, pp. 209–228, 2015.

[29] G. Chirikjian, *Stochastic Models, Information Theory, and Lie Groups, Volume 1*. Birkhäuser, 2009.

[30] F. Dellaert and M. Kaess, “Factor Graphs for Robot Perception,” *Foundations and Trends in Robotics*, vol. 6, no. 1-2, pp. 1–139, 2017.

[31] S. Nobili, G. Tinchev, and M. Fallon, “Predicting Alignment Risk to Prevent Localization Failure,” in *International Conference on Robotics and Automation (ICRA)*. IEEE, 2018, pp. 1003–1010.